RESEARCH ARTICLE

WILEY

Unsymmetric extensions of Wilson's incompatible four-node quadrilateral and eight-node hexahedral elements

Ying-Qing Huang[1] | Yuan-Fan Yang[1] | Ji-Zhen Wang[2] | Xiao-Chuan Liu[2] |
Hai-Bo Chen[1]

[1]CAS Key Laboratory of Mechanical Behavior and Design of Materials, Department of Modern Mechanics, University of Science and Technology of China, Hefei, China

[2]Aviation Key Laboratory of Science and Technology on Structure Impact Dynamics, Aircraft Strength Research Institute of China, Xian, China

Correspondence
Ying-Qing Huang and Hai-Bo Chen, CAS Key Laboratory of Mechanical Behavior and Design of Materials, Department of Modern Mechanics, University of Science and Technology of China, Hefei, Anhui 230027, China.
Email: yqhuang@ustc.edu.cn and hbchen@ustc.edu.cn

Abstract

The unsymmetric finite element is based on the virtual work principle with different sets of test and trial functions. In this article, the incompatible four-node quadrilateral element and eight-node hexahedral element originated by Wilson et al. are extended to their unsymmetric forms. The isoparametric shape functions together with Wilson's incompatible functions are chosen as the test functions, while internal nodes at the middle of element sides/edges are added to generate the trial functions with quadratic completeness in the Cartesian coordinate system. A local area/volume coordinate frame is established so that the trial shape functions can be explicitly obtained. The key idea which avoids the matrix inversion is that the trial nodal shape functions are constructed by standard quadratic triangular/tetrahedral elements and then transformed in consistent with the quadrilateral/hexahedral elements. Numerical examples show that the present elements keep the merits of both incompatible and unsymmetric elements, that is, high numerical accuracy, insensitivity to mesh distortion, free of trapezoidal and volumetric locking, and easy implementation.

KEYWORDS

finite element, incompatible finite element, mesh distortion, patch test condition, unsymmetric finite element method

1 | INTRODUCTION

With the progress of computer technology, the finite element method (FEM) has become one of the significant computation and simulation tools. It has been successfully and widely applied to various science and engineering problems. At the same time, many new methods have been adopted to develop high-performance finite elements. The word 'high-performance' means high numerical accuracy under coarse meshes, insensitivity to mesh distortion, and locking free, and so forth. In particular, developing high-performance low-order elements remains a constant challenge for researchers. Recent studies have shown the potential advantages of the unsymmetric FEM in this field.

The unsymmetric FEM proposed by Rajendran and Liew[1] is based on the virtual work principle and uses different sets of test and trial functions. Numerical examples have shown its excellent immunity to mesh distortion. Using the 8-node

unsymmetric finite element US-QUAD8,[1] the accurate analytical solutions of linear bending problems can be reproduced under severely distorted meshes. In the formulation of the unsymmetric element US-QUAD8, the test functions are standard isoparametric shape functions that are continuous at the element interfaces but only quadratic complete in the local coordinate frame. The trial shape functions are quadratic complete in the global Cartesian coordinate system but the inter-continuity requirements are not satisfied for distorted meshes. By selecting two different sets of shape functions defined in the local and global coordinate systems, respectively, the Jacobian determinant disappears from the formula of the element stiffness matrix. In summary, the virtual displacement continuity, global quadratic completeness of the actual displacements, and disappearance of Jacobian determinant[2] explain the high performance of the US-QUAD8 element.

Thereafter, the unsymmetric FEM is successfully extended to a 9-node quadrilateral element,[2] 6-node triangular element,[3] and a 20-node solid hexahedral element.[4] In all the above unsymmetric elements, their trial shape functions are obtained from polynomial basis functions expressed in terms of Cartesian coordinates. The above-mentioned unsymmetric elements have two main drawbacks: (1) they degenerate to conventional isoparametric elements when elements are not distorted. In other words, no improvements for regular meshes. (2) It is difficult to extend them to low-order elements because the quadratic completeness in the Cartesian coordinates cannot be satisfied due to the limitation of nodal degrees of freedom (DOF). For example, the 4-node quadrilateral element can only provide 4 DOFs in the x-direction, while the displacement in the x-direction needs at least six parameters to ensure the quadratic completeness.

Cen et al.[5] successfully developed a new unsymmetric 8-node element called US-ATFQ8 by applying the fundamental Airy stress solutions as the basis functions to obtain the trial shape functions. The US-ATFQ8 element can achieve fourth-order completeness of displacements in terms of Cartesian coordinates and therefore improve the numerical accuracy in comparison with the US-QUAD8 element. Later, Cen et al.[6] developed an unsymmetric 4-node quadrilateral element by adopting the fundamental analytical solutions expressed in the quadrilateral area coordinates. The unsymmetric 8-node hexahedral element[7] is also developed by applying Airy fundamental solutions similarly. Xie et al.[8] presented the unsymmetric 4-node quadrilateral and 8-node hexahedral elements by introducing the Trefftz stress solution to obtain the trial functions. An unsymmetric 4-node quadrilateral membrane element with the drilling DOFs is also developed by Shang et al.[9,10] The above unsymmetric elements depend on the fundamental Airy or Trefftz stress solutions and the assumed displacement components are coupled with each other.

In our previous work,[11] an unsymmetric 4-node quadrilateral element IUQ4 with incompatible internal displacements is proposed. Five internal nodes are added in the IUQ4 element to ensure the global quadratic completeness of the assumed actual displacements in the same way as the US-QUAD9 element.[2] The IUQ4 element exhibits very good numerical performance like other unsymmetric elements above and provides a new way to develop unsymmetric elements. Unfortunately, compared to other elements, the IUQ4 element is a bit time-consuming since it requires 3×3 Gaussian integration points to calculate the elemental stiffness matrix. Further investigations on the IUQ4 show that the internal central node may coincide with the actual nodes when the mesh is distorted in some special cases. The coincidence of nodal positions can lead to the failure of trial interpolation functions.

In this article, a novel unsymmetric 4-node quadrilateral element UQ6 is presented by introducing Wilson's incompatible functions[15] to the standard isoparametric test functions. The nonconforming test functions are revised to pass the constant stress patch test.[13] Two internal nodes at the mid-sides are added to obtain the trial shape functions. In contrast with the IUQ4 element, the present UQ6 element adopts the minimum number of internal nodes to ensure the requirement of the global quadratic completeness of the assumed displacements. Since the mid-sides are always unique to four corner nodes, the coincidence of nodal positions is avoided. The matrix to form the trial nodal shape functions is carefully studied and the calculation of the inverse matrix is ensured. Additionally, by introducing the local area coordinate system, explicit trial nodal shape functions can be obtained. Numerical results demonstrate the high performance of the present UQ6 element that only 2×2 Gaussian integration rule is required. The UQ6 element has good immunity to mesh distortion, rotational frame invariance, is free of trapezoidal locking, and easy to implementation.

Further, the three-dimensional incompatible Wilson element H11 [15] is also extended to its unsymmetric formulation, and the new incompatible unsymmetric 8-node hexahedral elements named UH11 is developed. The present element has three internal nodes at mid-edges and only a $2 \times 2 \times 2$ Gaussian integration rule is required. A local skew frame is constructed in the element central to secure the rotation invariance, while, a local volume coordinate system is introduced to obtain the nodal trial shape functions explicitly. Numerical examples indicate that the present element can pass the patch test and keep the rotation frame invariance. It also exhibit good convergence and excellent insensitivity to various severe mesh distortions as predicted.

2 | GENERAL FORMULATION AND IMPLEMENTATION OF UNSYMMETRIC FINITE ELEMENT

The unsymmetric FEM is established based on the virtual work principle in its discretization form as follows[1]:

$$\sum_e \left(\int_{V^e} \left(\delta\boldsymbol{\varepsilon}^T \boldsymbol{\sigma} - \delta\boldsymbol{u}^T \boldsymbol{f} \right) dV - \int_{S^e_\sigma} \delta\boldsymbol{u}^T \boldsymbol{T} dS \right) = 0 \tag{1}$$

in which e denotes elements. $\delta\boldsymbol{u}, \delta\boldsymbol{\varepsilon}$, and $\boldsymbol{\sigma}$ are the virtual displacement, virtual strain and actual stress, respectively. $\boldsymbol{f}$ is the body force in the element domain V^e and $\boldsymbol{T}$ is the surface traction on the boundary S^e_σ.

Using the stress–strain relationship and strain–displacement relationship, we have:

$$\boldsymbol{\varepsilon} = \boldsymbol{L}(\boldsymbol{u}), \boldsymbol{\sigma} = \boldsymbol{D}\boldsymbol{\varepsilon}, \delta\boldsymbol{\varepsilon} = \boldsymbol{L}(\delta\boldsymbol{u}) \tag{2}$$

where $\boldsymbol{D}$ is the material constitutive matrix and $\boldsymbol{L}$ is the differential operator matrix which always contains derivatives to the Cartesian coordinates.

Thereafter, the virtual displacement $\delta\boldsymbol{u}$ and the actual displacement $\boldsymbol{u}$ are approximated with nodal unknowns by:

$$\delta\boldsymbol{u} = \boldsymbol{N}\delta\boldsymbol{a}^e, \boldsymbol{u} = \boldsymbol{M}\boldsymbol{a}^e \tag{3}$$

where $\boldsymbol{N}$ and $\boldsymbol{M}$ are called the test and trial function matrices of nodal shape functions, respectively. $\boldsymbol{a}^e$ is the nodal displacement vector of the element.

Substituting Equation (3) into Equation (2) gives

$$\delta\boldsymbol{\varepsilon} = \boldsymbol{L}(\delta\boldsymbol{u}) = \boldsymbol{L}(\boldsymbol{N})\delta\boldsymbol{a}^e = \boldsymbol{B}\delta\boldsymbol{a}^e,$$
$$\boldsymbol{\sigma} = \boldsymbol{D}\boldsymbol{\varepsilon} = \boldsymbol{D}\boldsymbol{L}(\boldsymbol{u}) = \boldsymbol{D}\boldsymbol{L}(\boldsymbol{M})\boldsymbol{a}^e = \boldsymbol{D}\overline{\boldsymbol{B}}\boldsymbol{a}^e \tag{4}$$

in which $\boldsymbol{B}$ and $\overline{\boldsymbol{B}}$ are strain matrices corresponding to the test and trial nodal shape functions, respectively.

Substituting Equations (3) and (4) into Equation (1), one can establish the discrete equilibrium equations by the assembly. The details are omitted and we only give the element stiffness matrix as follows

$$\boldsymbol{K}^e = \int_{V^e} \boldsymbol{B}^T \boldsymbol{D}\overline{\boldsymbol{B}} dV \tag{5}$$

In the traditional FEM, the test and trial functions are usually selected from the same isoparametric shape functions which results in the symmetric element stiffness matrix. However, when the test and trial functions are different, we obtain the unsymmetric element stiffness matrix in Equation (5).

When $\boldsymbol{N}$ and $\boldsymbol{M}$ are defined in the natural and Cartesian coordinates, respectively, and the elemental integration is computed in the natural coordinate frame, the element stiffness matrix can be rewritten as

$$\boldsymbol{K}^e = \int_{-1}^{1} \int_{-1}^{1} \int_{-1}^{1} \boldsymbol{B}^T \boldsymbol{D}\overline{\boldsymbol{B}} |\boldsymbol{J}| d\xi d\eta d\zeta = \int_{-1}^{1} \int_{-1}^{1} \int_{-1}^{1} \boldsymbol{B}^{*T} \boldsymbol{D}\overline{\boldsymbol{B}} d\xi d\eta d\zeta \tag{6}$$

in which $\boldsymbol{B} = \boldsymbol{L}(\boldsymbol{N}(\xi, \eta, \zeta)) = \frac{\boldsymbol{B}^*}{|\boldsymbol{J}|}, \overline{\boldsymbol{B}} = \boldsymbol{L}(\boldsymbol{M}(x, y, z))$, and $|\boldsymbol{J}|$ is the Jacobian determinant. It is shown that the Jacobian determinant disappears in the computation of the element stiffness matrix. This is the key feature of the unsymmetric FEM.

The success of the US-QUAD8 element can be explained from three aspects as stated by Rajendran and Liew[1]:

a. The test function is continuous and compatible between the element interfaces.
b. The trial function is quadratic complete in the global coordinates, even when the mesh is distorted.
c. The unsymmetric element stiffness matrix can be exactly integrated through Gaussian integration since the Jacobian determinant is eliminated.

The traditional Q8 element satisfies the first requirement, while the next two conditions are ensured only for regular meshes. This explains why the Q8 element exhibits poor performance with mesh distortion. It should be emphasized that the condition (c) is very important and plays a key role in the unsymmetric FEM. When the Jacobian determinant equals zero, the conventional isoparametric elements fail to evaluate the element stiffness matrix or stresses at the sample points. However, the unsymmetric FEM can overcome it without any additional treatments.

Though the above unsymmetric FEM is very attractive, it is difficult to be extended to low-order elements since the inter-continuity and quadratic completeness requirements cannot be fulfilled simultaneously. In our previous work,[11] it is found that the inter-continuity requirement can be approximately satisfied and the proposed incompatible unsymmetric 4-noded element IUQ4 still shows very good numerical performance. Unfortunately, the IUQ4 element needs a 3×3 Gaussian integration rule and is therefore costly. Considering the symmetry, the IUQ4 element chooses five internal nodes and connects the nodal displacements with internal parameters. Further investigations show that this is not essential. In this article, we extend Wilson's plane and solid elements to their unsymmetric forms. A new method with a local area/volume coordinate frame established at the corner node is proposed to avoid the calculation of the inverse matrix and to give the trial shape functions explicitly.

3 | EXTENSION OF WILSON'S PLANE Q6 ELEMENT

3.1 | Element coordinate transformation and test shape functions

As shown in Figure 1, the Cartesian coordinates in a 4-noded quadrilateral element are expressed in terms of shape functions and nodal coordinates by

$$
\begin{Bmatrix} x \\ y \end{Bmatrix} = \sum_{i=1}^{4} \begin{bmatrix} N_i & 0 \\ 0 & N_i \end{bmatrix} \begin{Bmatrix} x_i \\ y_i \end{Bmatrix} = \begin{Bmatrix} a_1\xi + a_2\xi\eta + a_3\eta + a_4 \\ b_1\xi + b_2\xi\eta + b_3\eta + b_4 \end{Bmatrix}
\tag{7}
$$

where $N_i = \frac{1}{4}(1 + \xi_i\xi)(1 + \eta_i\eta)$, $i = 1, 2, 3, 4$ are nodal shape functions, and a_i, b_i are the geometric parameters defined by

$$
\begin{bmatrix} a_1 & b_1 \\ a_2 & b_2 \\ a_3 & b_3 \\ a_4 & b_4 \end{bmatrix} = \frac{1}{4} \begin{bmatrix} -1 & 1 & 1 & -1 \\ 1 & -1 & 1 & -1 \\ -1 & -1 & 1 & 1 \\ 1 & 1 & 1 & 1 \end{bmatrix} \begin{bmatrix} x_1 & y_1 \\ x_2 & y_2 \\ x_3 & y_3 \\ x_4 & y_4 \end{bmatrix}
\tag{8}
$$

The virtual displacement in the element is assumed to be

$$
\delta\boldsymbol{u} = \begin{Bmatrix} \delta u \\ \delta v \end{Bmatrix} = \sum_{i=1}^{4} \begin{bmatrix} N_i & 0 \\ 0 & N_i \end{bmatrix} \begin{Bmatrix} \delta u_i \\ \delta v_i \end{Bmatrix} + \sum_{i=5}^{6} \begin{bmatrix} N_i & 0 \\ 0 & N_i \end{bmatrix} \begin{Bmatrix} \delta u_i \\ \delta v_i \end{Bmatrix}
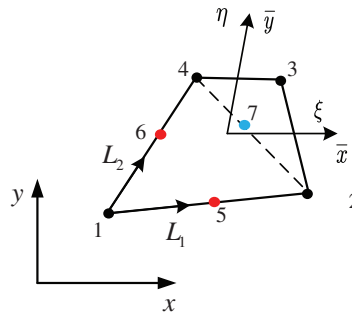\tag{9}
$$

FIGURE 1 Four-node element configuration with internal nodes

where δu_i and δv_i are the virtual nodal displacements ($i = 1, 2, 3, 4$) and the virtual internal DOF ($i = 5, 6$), respectively. The nodal shape functions are defined the same as in Equation (7). The shape functions associated with the internal DOFs are the same as those of Wilson's Q6 element, that is,

$$N_5 = 1 - \xi^2, \quad N_6 = 1 - \eta^2 \tag{10}$$

It is noted that the approximation of the element virtual displacements is composed of the standard isoparametric four-node bilinear interpolation and the incompatible quadratic terms. The incompatible shape functions in Equation (10) is originally proposed by Wilson et al.[15] to develop the incompatible element Q6.

3.2 | Trial shape functions with the skew coordinate frame

To construct the trial nodal shape functions, we should add two internal nodes in consistent with the test internal DOFs. Two neighboring mid-side nodes are selected as the internal nodes as shown in Figure 1. Thereafter, the trial shape functions of the six nodes can be computed in the same way as in the reference article 1. However, to secure the rotation invariance and isotropy in the element, a local skew coordinate frame suggested by Yuan et al.[12] is established in the center of the element. The coordinate transformation between the global and skew frames is expressed as

$$\begin{Bmatrix} \bar{x} \\ \bar{y} \end{Bmatrix} = \begin{bmatrix} \frac{\partial \xi}{\partial x} & \frac{\partial \xi}{\partial y} \\ \frac{\partial \eta}{\partial x} & \frac{\partial \eta}{\partial y} \end{bmatrix}_{\xi=\eta=0} \begin{Bmatrix} x - a_4 \\ y - b_4 \end{Bmatrix} = \boldsymbol{J}^{-T}\big|_{\xi=\eta=0} \begin{Bmatrix} x - a_4 \\ y - b_4 \end{Bmatrix} \tag{11}$$

where (a_4, b_4) are the coordinates of the element center and $\boldsymbol{J}^{-T}\big|_{\xi=\eta=0}$ indicates the inverse and transpose of the Jacobian matrix computed at the element center. It can be explicitly represented by the geometric parameters defined in Equation (8)

$$\begin{Bmatrix} \bar{x} \\ \bar{y} \end{Bmatrix} = \frac{1}{J_0} \begin{bmatrix} b_3 & -a_3 \\ -b_1 & a_1 \end{bmatrix} \begin{Bmatrix} x - a_4 \\ y - b_4 \end{Bmatrix}, \quad J_0 = a_1 b_3 - a_3 b_1 \tag{12}$$

The above skew frame ($\bar{x}, \bar{y}$) is coincident with the natural frame (ξ, η) at the element center. It has been verified that the trial functions based on the local skew coordinates can ensure the rotation invariance and isotropy of the element.[8] The trial nodal shape functions defined in the skew frame can be obtained by satisfying the following equations[1]:

$$\begin{bmatrix} 1 & 1 & 1 & 1 & 1 & 1 \\ \bar{x}_1 & \bar{x}_2 & \bar{x}_3 & \bar{x}_4 & \bar{x}_5 & \bar{x}_6 \\ \bar{y}_1 & \bar{y}_2 & \bar{y}_3 & \bar{y}_4 & \bar{y}_5 & \bar{y}_6 \\ \bar{x}_1^2 & \bar{x}_2^2 & \bar{x}_3^2 & \bar{x}_4^2 & \bar{x}_5^2 & \bar{x}_6^2 \\ \bar{y}_1^2 & \bar{y}_2^2 & \bar{y}_3^2 & \bar{y}_4^2 & \bar{y}_5^2 & \bar{y}_6^2 \\ \bar{x}_1\bar{y}_1 & \bar{x}_2\bar{y}_2 & \bar{x}_3\bar{y}_3 & \bar{x}_4\bar{y}_4 & \bar{x}_5\bar{y}_5 & \bar{x}_6\bar{y}_6 \end{bmatrix} \begin{Bmatrix} M_1 \\ M_2 \\ M_3 \\ M_4 \\ M_5 \\ M_6 \end{Bmatrix} = \begin{Bmatrix} 1 \\ \bar{x} \\ \bar{y} \\ \bar{x}^2 \\ \bar{y}^2 \\ \overline{xy} \end{Bmatrix} \tag{13}$$

Unfortunately, the inverse of the above coefficient matrix may be unsuccessful when the element becomes a triangle, or its two neighboring sides coincide. To overcome this difficulty, a pre-computation is needed to check whether the element degenerates to a triangle or not. One can compute the absolute areas of the four triangles, $\triangle 124$, $\triangle 231$, $\triangle 342$, and $\triangle 413$ or the Jacobian determinant at the four nodes to find the zero value. Considering the computer float errors, we only find the absolute minimum value. For example, assuming $\triangle 342$ is the minimum, its diagonal node 1 is chosen as the joint of the two neighboring sides with internal nodes 5 and 6 as shown in Figure 1. In this case, only the area of the triangle $\triangle 342$ may be zero. Note that the internal node 5 always lays at the middle of side 1–2 or 3–4, while node 6 in the side 2–3 or 1–4. This selection is consistent with the test incompatible shape function defined in Equation (10). In the following formulation, $\triangle 342$ is assumed the minimum and is the only one which may be a zero triangle.

Applying the skew coordinate transformation by Equation (12), the coefficient matrix in Equation (13) can be expressed as:

$$
\boldsymbol{P}_M = \begin{bmatrix}
1 & 1 & 1 & 1 & 1 & 1 \\
-1+\beta & 1-\beta & 1+\beta & -1-\beta & 0 & -1 \\
-1+\alpha & -1-\alpha & 1+\alpha & 1-\alpha & -1 & 0 \\
(1-\beta)^2 & (1-\beta)^2 & (1+\beta)^2 & (1+\beta)^2 & 0 & 1 \\
(1-\alpha)^2 & (1+\alpha)^2 & (1+\alpha)^2 & (1-\alpha)^2 & 1 & 0 \\
(1-\beta)(1-\alpha) & -(1-\beta)(1+\alpha) & (1+\beta)(1+\alpha) & -(1+\beta)(1-\alpha) & 0 & 0
\end{bmatrix}
\tag{14}
$$

where $\alpha = \frac{J_1}{J_0}$, $\beta = \frac{J_2}{J_0}$, $J_1 = a_1 b_2 - a_2 b_1$, $J_2 = a_2 b_3 - a_3 b_2$. The determinant of the above matrix is $|\boldsymbol{P}_M| = -16(1 - \alpha + \beta)(1 + \alpha - \beta)(1 - \alpha - \beta)^2$. Note the Jacobian determinant at any point is $|\boldsymbol{J}(\xi, \eta)| = J_0(1 + \alpha\xi + \beta\eta)$. Therefore, we have

$$
|\boldsymbol{P}_M| = -16|\boldsymbol{J}(-1, 1)| \cdot |\boldsymbol{J}(1, -1)| \cdot |\boldsymbol{J}(-1, -1)|^2 / J_0^4 \neq 0
$$

This explains that the determinant is the multiply of areas of the three triangles $\triangle413$, $\triangle231$, and $\triangle124$ which are not zeros. The matrix $\boldsymbol{P}_M$ is invertible and the explicit nodal shape functions can be obtained by the mathematic software. Due to the complication of the explicit expressions, they are not provided here.

3.3 | Trial shape functions with area coordinate frame

In the previous section, based on the skew frame and careful selections of the additional internal nodes, we obtain the trial nodal shape functions by the calculation of the inverse matrix $\boldsymbol{P}_M$. Although the explicit expressions can be given, they are relatively complicated.

In this section, a local area coordinate system is established and the actual displacement of the element is assumed in the area coordinates. First, the pre-computation the same as in the previous section is implemented to determine the positions of the two internal nodes. As shown in Figure 1, we still assume $\triangle342$ is the minimum. Then, the local area coordinate system (L_1, L_2) is constructed through $\triangle124$. The local coordinate of the nodes 1, 2, and 4 are $(0, 0)$, $(1, 0)$, and $(0, 1)$, respectively. The coordinate transformation between the global Cartesian and local area frames can be expressed as

$$
\begin{Bmatrix} x \\ y \\ 1 \end{Bmatrix} = \begin{bmatrix} x_2 & x_4 & x_1 \\ y_2 & y_4 & y_1 \\ 1 & 1 & 1 \end{bmatrix} \begin{Bmatrix} L_1 \\ L_2 \\ L_3 \end{Bmatrix}
\tag{15}
$$

Note that the coordinate transformation is linear and the completeness of the assumed displacement in both coordinate frames is identical. It is emphasized that the area coordinates are not limited to [0,1].

Considering the quadratic triangular element with six nodes 1, 2, 4, 5, 6, and 7, the displacement component can be assumed as:

$$
u = \overline{M}_1 u_1 + \overline{M}_2 u_2 + \overline{M}_4 u_4 + \overline{M}_5 u_5 + \overline{M}_6 u_6 + \overline{M}_7 u_7
\tag{16}
$$

where

$$
\overline{M}_1 = 2L_3^2 - L_3, \overline{M}_2 = 2L_1^2 - L_1, \overline{M}_4 = 2L_2^2 - L_2, \overline{M}_5 = 4L_1 L_3, \overline{M}_6 = 4L_2 L_3, \overline{M}_7 = 4L_1 L_2.
$$

The assumed displacement is quadratic complete in the global coordinate system and the nodal shape functions satisfy the Kronecker delta property. The node 7 is temporary and should be replaced. By substituting the area coordinate of node 3 into Equation (16), we have

$$u_3 = \overline{M}_1\big|_3 u_1 + \overline{M}_2\big|_3 u_2 + \overline{M}_4\big|_3 u_4 + \overline{M}_5\big|_3 u_5 + \overline{M}_6\big|_3 u_6 + \overline{M}_7\big|_3 u_7 \tag{17}$$

where $\overline{M}_i\big|_3$ means the value of the shape function $\overline{M}_i$ at node 3. Note that $\overline{M}_7\big|_3$ is zero only when the sides 1–2 and 2–3 or 2–3 and 3–4 coincide. Since the triangle $\triangle 342$ is the minimum, this will not happen. By replacing u_7 with u_3, we finally obtain the trial nodal shape functions as follows:

$$M_3 = \frac{1}{\overline{M}_7\big|_3}\overline{M}_7, M_i = \overline{M}_i - \overline{M}_i\big|_3 M_3, (i = 1, 2, 4, 5, 6).$$

It is observed that the present method provides a very straightforward way to form the explicit trial nodal shape functions without matrix inversion. Two main steps are included. First, the standard nodal shape functions of a 6-node quadratic triangular element are formed. Since the triangle is straight-edged, the global quadratic completeness of shape functions can be ensured. Second, the nodal shape functions are transformed to be consistent with the 4-node quadrilateral element with two internal nodes.

3.4 | Elemental stiffness matrix and static condensation

After obtaining trial nodal shape functions, the elemental actual displacement is then approximated by

$$\boldsymbol{u} = \begin{Bmatrix} u \\ v \end{Bmatrix} = \sum_{i=1}^{6} \begin{bmatrix} M_i & 0 \\ 0 & M_i \end{bmatrix} \begin{Bmatrix} u_i \\ v_i \end{Bmatrix} \tag{18}$$

Since the relationship in Equation (12) between the local skew and Cartesian coordinates is always linear, the global quadratic completeness of trial functions can be maintained. From the approximations of virtual and actual displacements in Equations (3) and (4), we can obtain the element stiffness matrix and nodal equivalent force vector as discussed in the previous section.

The initial 12×12 unsymmetric element stiffness matrix defined in Equation (5) is numerically computed by Gaussian integration. Then, a static condensation is implemented to form the final 8×8 unsymmetric element stiffness matrix.

The detailed process of static condensation is provided as below. First, the strain matrix $\boldsymbol{B}$ corresponding to the test shape functions is divided into two sub-matrices,

$$\boldsymbol{B} = \begin{bmatrix} \boldsymbol{B}_q & \boldsymbol{B}_\lambda \end{bmatrix} \tag{19}$$

where $\boldsymbol{B}_q$ and $\boldsymbol{B}_\lambda$ are respectively, related to the elemental nodal displacements and the internal DOFs. The same division is also applied to the strain matrix $\overline{\boldsymbol{B}}$ corresponding to the trial functions. Therefore, the initial 12×12 unsymmetric element stiffness matrix can be rearranged as

$$\boldsymbol{K}^e = \int_{V^e} \begin{bmatrix} \boldsymbol{B}_q & \boldsymbol{B}_\lambda \end{bmatrix}^T \boldsymbol{D} \begin{bmatrix} \overline{\boldsymbol{B}}_q & \overline{\boldsymbol{B}}_\lambda \end{bmatrix} dV = \begin{bmatrix} \boldsymbol{K}^e_{qq} & \boldsymbol{K}^e_{q\lambda} \\ \boldsymbol{K}^e_{\lambda q} & \boldsymbol{K}^e_{\lambda\lambda} \end{bmatrix} \tag{20}$$

where

$$\boldsymbol{K}^e_{qq} = \int_{V^e} \boldsymbol{B}^T_q \boldsymbol{D}\overline{\boldsymbol{B}}_q dV, \boldsymbol{K}^e_{q\lambda} = \int_{V^e} \boldsymbol{B}^T_q \boldsymbol{D}\overline{\boldsymbol{B}}_\lambda dV, \boldsymbol{K}^e_{\lambda q} = \int_{V^e} \boldsymbol{B}^T_\lambda \boldsymbol{D}\overline{\boldsymbol{B}}_q dV, \boldsymbol{K}^e_{\lambda\lambda} = \int_{V^e} \boldsymbol{B}^T_\lambda \boldsymbol{D}\overline{\boldsymbol{B}}_\lambda dV$$

It is noted that the internal DOF are defined within each element and can be eliminated from the following partition equilibrium equation

$$\begin{bmatrix} \boldsymbol{K}^e_{qq} & \boldsymbol{K}^e_{q\lambda} \\ \boldsymbol{K}^e_{\lambda q} & \boldsymbol{K}^e_{\lambda\lambda} \end{bmatrix} \begin{Bmatrix} \boldsymbol{a}_q \\ \lambda \end{Bmatrix} = \begin{Bmatrix} \boldsymbol{P}_q \\ 0 \end{Bmatrix} \tag{21}$$

or, equivalently,

$$\begin{cases} \boldsymbol{K}_{qq}^e \boldsymbol{a}_q + \boldsymbol{K}_{q\lambda}^e \lambda = \boldsymbol{P}_q \\ \boldsymbol{K}_{\lambda q}^e \boldsymbol{a}_q + \boldsymbol{K}_{\lambda\lambda}^e \lambda = 0 \end{cases} \tag{22}$$

where $\boldsymbol{P}_q$ is the nodal force vector which includes the external consistent equivalent nodal load vector and the internal force by the adjacent elements. According to the second equilibrium equation in Equation (22), the internal nodal displacement λ can be solved:

$$\lambda = -\left(\boldsymbol{K}_{\lambda\lambda}^e\right)^{-1} \boldsymbol{K}_{\lambda q}^e \boldsymbol{a}_q \tag{23}$$

Introducing Equation (23) into the first equation in Equation (22) results in

$$\boldsymbol{K}^{*e} \boldsymbol{a}_q = \boldsymbol{P}_q \tag{24}$$

where $\boldsymbol{K}^{*e} = \boldsymbol{K}_{qq}^e - \boldsymbol{K}_{q\lambda}^e \left(\boldsymbol{K}_{\lambda\lambda}^e\right)^{-1} \boldsymbol{K}_{\lambda q}^e$ is the resulted 8×8 unsymmetric element stiffness matrix.

To ensure the convergence of the element, Wilson's internal test shape functions should be modified to pass the patch test. In this article, the modification in the NQ6 element[13] or the revision method IV in the literature 14 is adopted. The explicit formulations are given by

$$N_5^* = N_5 + \frac{2}{3}(\alpha\xi - \beta\eta), \quad N_6^* = N_6 - \frac{2}{3}(\alpha\xi - \beta\eta)$$

where N_i^* are the revised incompatible test shape functions.

Since the actual displacement are both quadratic complete, the resulted elements based on the local skew or area coordinate frames are equivalent. We denote this unsymmetric element as UQ6 in comparison with Wilson's Q6 element.

4 | EXTENSION OF WILSON'S SOLID H11 ELEMENT

In analogous to the UQ6 element, incompatible internal displacements and internal nodes are introduced into test and trial interpolation functions to construct the new unsymmetric 8-node hexahedral element UH11. As shown in Figure 2, three internal nodes located in the midpoints of the three neighboring edges are added to a standard hexahedral element.

The virtual displacements composed of virtual nodal displacements and virtual internal DOFs are assumed as:

$$\delta u = \begin{Bmatrix} \delta u \\ \delta v \\ \delta w \end{Bmatrix} = \sum_{i=1}^{8} \begin{bmatrix} N_i & 0 & 0 \\ 0 & N_i & 0 \\ 0 & 0 & N_i \end{bmatrix} \begin{Bmatrix} \delta u_i \\ \delta v_i \\ \delta w_i \end{Bmatrix} + \sum_{i=9}^{11} \begin{bmatrix} N_i & 0 & 0 \\ 0 & N_i & 0 \\ 0 & 0 & N_i \end{bmatrix} \begin{Bmatrix} \delta u_i \\ \delta v_i \\ \delta w_i \end{Bmatrix} \tag{25}$$

where the shape functions associated with actual nodes and the internal DOFs are listed below:
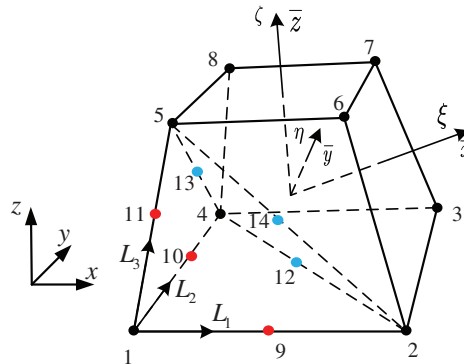

FIGURE 2 Eight-node element configuration with internal nodes

$$N_i = \frac{1}{8} (1 + \xi_i \xi)(1 + \eta_i \eta)(1 + \zeta_i \zeta), i = 1 \sim 8$$

$$N_9 = 1 - \xi^2, N_{10} = 1 - \eta^2, N_{11} = 1 - \zeta^2$$

in which N_i ($i = 1 \sim 8$) are the shape functions of the traditional 8-node tri-linear isoparametric hexahedral element, and N_i ($i = 9 \sim 11$) are the same as those of Wilson's incompatible element H11.[15] The approximate virtual displacement is quadratic complete in the natural coordinate frame after the introduction of incompatible quadratic terms.

Three neighboring mid-side nodes are selected as the internal nodes to construct the trial nodal shape functions. In the same way, as in the previous section, pre-computation is done to decide the corner node where the three neighboring sides join together. At each corner node, a tetrahedron containing the corner's three neighboring sides is formed and its volume is calculated. We find the absolute minimum of volumes from the eight tetrahedrons and choose its diagonal corner node as the one for use. As shown in Figure 2, the corner node 1 is selected, this implies that the tetrahedron T7386 is the minimum. It should be mentioned that the three internal nodes 9, 10, and 11 are required to locate at the sides along ξ, η, and ζ directions, respectively, in consistent with the incompatible test functions N_i ($i = 9 \sim 11$).

The local skew coordinate and volume coordinate frames are both used to evaluate the trial nodal shape functions. As in the previous section, the coordinate transformation between the physical and skew frames can be written as:

$$\left\{ \begin{matrix} \bar{x} \\ \bar{y} \\ \bar{z} \end{matrix} \right\} = \boldsymbol{J}^{-T}\big|_{\xi=\eta=\zeta=0} \left(\left\{ \begin{matrix} x \\ y \\ z \end{matrix} \right\} - \left\{ \begin{matrix} x \\ y \\ z \end{matrix} \right\}\bigg|_{\xi=\eta=\zeta=0} \right) \tag{26}$$

where $\boldsymbol{J}^{-T}$ indicates the inverse and transpose of the Jacobian matrix.

The nodal trial shape functions defined in the local skew coordinates can be solved by the following linear algebraic equations:

$$\begin{bmatrix} 1 & 1 & \cdots & 1 & 1 \\ \bar{x}_1 & \bar{x}_2 & \cdots & \bar{x}_{10} & \bar{x}_{11} \\ \bar{y}_1 & \bar{y}_2 & \cdots & \bar{y}_{10} & \bar{y}_{11} \\ \bar{z}_1 & \bar{z}_2 & \cdots & \bar{z}_{10} & \bar{z}_{11} \\ \bar{x}_1^2 & \bar{x}_2^2 & \cdots & \bar{x}_{10}^2 & \bar{x}_{11}^2 \\ \bar{x}_1\bar{y}_1 & \bar{x}_2\bar{y}_2 & \cdots & \bar{x}_{10}\bar{y}_{10} & \bar{x}_{11}\bar{y}_{11} \\ \bar{y}_1^2 & \bar{y}_2^2 & \cdots & \bar{y}_{10}^2 & \bar{y}_{11}^2 \\ \bar{y}_1\bar{z}_1 & \bar{y}_2\bar{z}_2 & \cdots & \bar{y}_{10}\bar{z}_{10} & \bar{y}_{11}\bar{z}_{11} \\ \bar{z}_1^2 & \bar{z}_2^2 & \cdots & \bar{z}_{10}^2 & \bar{z}_{11}^2 \\ \bar{x}_1\bar{z}_1 & \bar{x}_2\bar{z}_2 & \cdots & \bar{x}_{10}\bar{z}_{10} & \bar{x}_{11}\bar{z}_{11} \\ \bar{x}_1\bar{y}_1\bar{z}_1 & \bar{x}_2\bar{y}_2\bar{z}_2 & \cdots & \bar{x}_{10}\bar{y}_{10}\bar{z}_{10} & \bar{x}_{11}\bar{y}_{11}\bar{z}_{11} \end{bmatrix} \left\{ \begin{matrix} M_1 \\ M_2 \\ M_3 \\ M_4 \\ M_5 \\ M_6 \\ M_7 \\ M_8 \\ M_9 \\ M_{10} \\ M_{11} \end{matrix} \right\} = \left\{ \begin{matrix} 1 \\ \bar{x} \\ \bar{y} \\ \bar{z} \\ \bar{x}^2 \\ \overline{xy} \\ \bar{y}^2 \\ \overline{yz} \\ \bar{z}^2 \\ \overline{xz} \\ \overline{xyz} \end{matrix} \right\} \tag{27}$$

Unlike in the 2D case, it is difficult to calculate the determinant of the above coefficient matrix explicitly. Therefore, one cannot ensure the matrix is not singular for any distorted element.

To prove the coefficient matrix in Equation (27) is invertible and for obtaining the explicit nodal shape functions, the local volume coordinate frame (L_1, L_2, L_3) is built. The volume coordinate is usually applied in the isoparametric tetrahedral elements. The linear transformation from the local volume coordinate to the global coordinate takes the form of

$$\left\{ \begin{matrix} x \\ y \\ z \\ 1 \end{matrix} \right\} = \begin{bmatrix} x_2 & x_4 & x_5 & x_1 \\ y_2 & y_4 & y_5 & y_1 \\ z_2 & z_4 & z_5 & z_1 \\ 1 & 1 & 1 & 1 \end{bmatrix} \left\{ \begin{matrix} L_1 \\ L_2 \\ L_3 \\ L_4 \end{matrix} \right\} \tag{28}$$

As shown in Figure 2, the tetrahedron T2451 is adopted since the volume of the diagonal tetrahedron T8637 is pre-computed to be the minimum. Here, we assume that the T8637 is the only one which may be a zero tetrahedron in the following formulation. The volume coordinates of the four nodes 2, 5, 4, and 1, are (1, 0, 0), (0, 1, 0), (0, 0, 1), and (0, 0, 0), respectively. Note that the volume coordinate is not restricted to the closed interval [0,1].

The element displacement component is interpolated by a 10-node tetrahedral element (node 2, 5, 4, 1, 9, 10, 11, 12, 13, 14 as shown in Figure 2) with an additional cubic term as follows:

$$u = \overline{M}_7 \beta_7 + \sum_i \overline{M}_i u_i, \quad (i = 1, 2, 4, 5, 9, 10, 11, 12, 13, 14) \tag{29}$$

where

$$\overline{M}_1 = 2L_4^2 - L_4, \overline{M}_2 = 2L_1^2 - L_1, \overline{M}_4 = 2L_2^2 - L_2, \overline{M}_5 = 2L_3^2 - L_3, \overline{M}_9 = 4L_1L_4,$$

$$\overline{M}_{10} = 4L_2L_4, \overline{M}_{11} = 4L_3L_4, \overline{M}_{12} = 4L_1L_2, \overline{M}_{13} = 4L_2L_3, \overline{M}_{14} = 4L_1L_3,$$

$$\overline{M}_7 = \overline{xyz} - \sum_i \overline{x}_i \overline{y}_i \overline{z}_i \overline{M}_i, \quad (i = 1, 2, 4, 5, 9, 10, 11, 12, 13, 14)$$

The introduction of $\overline{M}_7$ ensure the assumed displacement in Equation (29) is quadratic complete in the global coordinate system and is equivalent to Equation (27). Note that $\overline{x}_i, \overline{y}_i, \overline{z}_i$ in $\overline{M}_7$ are nodal coordinates in the local skew frame defined in Equation (26). It is demonstrated that $\overline{M}_7$ has no effect on the Kronecker delta property of other nodal shape functions. By substituting the coordinates of node 7 into Equation (29), we have

$$u_7 = \overline{M}_7 \big|_7 \beta_7 + \sum_i \overline{M}_i \big|_7 u_i, \quad (i = 1, 2, 4, 5, 9, 10, 11, 12, 13, 14) \tag{30}$$

where $\overline{M}_i \big|_7$ means the value of the shape function $\overline{M}_i$ at node 7 which is nonzero. By eliminating β_7 using Equation (30), the assumed displacement can be rewritten as

$$u = \frac{\overline{M}_7}{\overline{M}_7 \big|_7} u_7 + \sum_i \left(\overline{M}_i - \frac{\overline{M}_i \big|_7}{\overline{M}_7 \big|_7} \overline{M}_7 \right) u_i, \quad (i = 1, 2, 4, 5, 9, 10, 11, 12, 13, 14) \tag{31}$$

The intermediate nodal displacements u_{12}, u_{13}, and u_{14} can be replaced by u_3, u_8, and u_6, similarly. Finally, we have the assumed displacement as follows

$$u = \sum_{i=1}^{11} M_i u_i \tag{32}$$

The explicit expressions of the nodal shape functions M_i are omitted due to complication. It should be mentioned that $\overline{M}_7$ can be substituted by the cubic term $L_1 L_2 L_3$ and the resulted element has a minor difference with the former.

The elemental actual displacements with quadratic completeness are approximated by

$$\boldsymbol{u} = \begin{Bmatrix} u \\ v \\ w \end{Bmatrix} = \sum_{i=1}^{11} \begin{bmatrix} M_i & 0 & 0 \\ 0 & M_i & 0 \\ 0 & 0 & M_i \end{bmatrix} \begin{Bmatrix} u_i \\ v_i \\ w_i \end{Bmatrix} \tag{33}$$

The introduction of local skew coordinates can ensure rotation invariance. The pre-computation and selections of internal nodes together with the introduction of volume coordinates can obtain the trial shape functions explicitly except that the hexahedral element is severely degenerated, for instance, two or more tetrahedrons at the corner have zero volumes.

Again, the initial 33×33 unsymmetric element stiffness matrix is reduced to 24×24 by static condensation before assembly. Similarly, the incompatible test shape functions N_i ($i = 9 \sim 11$) should be modified to pass the patch test. In this article, the modification by Wu et al.[13] is adopted in this article.

The resulted unsymmetric element is denoted as UH11 which can be regarded as a direct extension of Wilson's incompatible 3D element H11.

The present unsymmetric incompatible elements UQ6 and UH11 retain both advantages of the unsymmetric and incompatible elements. Since the test and trial interpolations are based on the natural and local frames, respectively, and the local frame is only a linear transformation of Cartesian coordinates, the Jacobian determinant can still be eliminated from the element stiffness matrix. Compared with the original unsymmetric FEM, this method relaxes the continuity requirement of the virtual displacement in the element interfaces. The present method also improves the numerical accuracy for regular meshes by the introduction of the incompatible trial and test functions.

The UQ6 element adopts the minimum number of internal nodes to ensure the global quadratic completeness of the assumed displacements. Due to careful selections of internal nodes and explicit trial shape functions, the present elements UQ6 and UH11 are much efficient and are easier to be generalized for solving other physical problems.

5 | NUMERICAL TESTS FOR THE 2D ELEMENT UQ6

In this section, the performance of the element denoted UQ6 is studied by some typical test problems. The elements adopted for comparison include some typical incompatible, hybrid, and recently developed unsymmetric elements. Except for the IUQ4 element which adopts a 3×3 Gaussian integration scheme, all other elements use a 2×2 integration scheme. The selected elements are listed below:

UQ6: present incompatible and unsymmetric element.
Q4: standard isoparametric element.
Q6: Incompatible element by Wilson.[15]
QM6: Incompatible element by Taylor et al.[16]
NQ6: Incompatible element by Wu et al.[13]
PS: Incompatible element by Pian and Sumihara.[17]
PS(α): Penalty equilibrium hybrid stress element by Wu et al.[18]
SPS: Scaled PS element by Sze.[19]
SYHP: Scaled YHP[12] element by Sze.[19]
IUQ4: Incompatible and unsymmetric element with five internal nodes by Huang et al.[11]
TQ4: Trefftz unsymmetric element by Xie et al.[8]
US-ATFQ4: unsymmetric element using Airy stress solution based on quadrilateral area coordinates by Cen et al.[6]

5.1 | Patch test and rotational invariance

The patch test prescribed by MacNeal and Harder[20] is a fundamental test for finite elements. The geometry, material properties are described in Figure 3. The model is divided into five arbitrary elements. The boundary conditions corresponding to the constant strain are

$$u = 10^{-3}(x + y/2) \quad v = 10^{-3}(y + x/2) \tag{34}$$

The theoretical solutions are

$$\sigma_x = \sigma_y = 1333; \quad \tau_{xy} = 400 \tag{35}$$

In our test, the present element UQ6 provides the exact solution and strictly passes the patch test. Especially, node 3 is re-positioned to (0.12,0.04) as the dotted-line shown in Figure 3. In this case, the patch contains three concave quadrilateral elements. Again, the present element has no difficulty to pass the constant stress test.
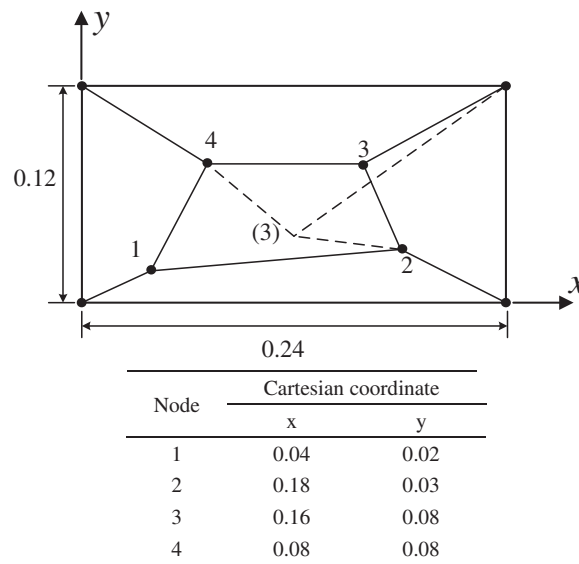
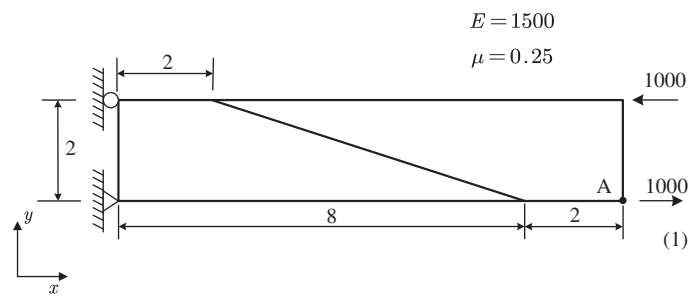**FIGURE 3** Patch test for plates, $E = 10^6$; $\nu = 0.25$

Node	Cartesian coordinate	
	x	y
1	0.04	0.02
2	0.18	0.03
3	0.16	0.08
4	0.08	0.08

FIGURE 4 Rotation dependence test

5.2 | Rotational frame dependence test

As shown in Figure 4, a cantilever beam divided by two distorted elements is subjected to pure moment. To test whether the UQ6 element is invariant and isotropic, the Cartesian coordinate system rotates counterclockwise from 0° to 90° in the step of 10° around the origin of coordinates. The displacement of point A along two axes is obtained and the magnitude of displacement $\sqrt{u_A^2 + v_A^2}$ is calculated. The results obtained by the new element UQ6 are given in Table 1. It can be seen that the present element UQ6 is invariant and isotropic.

5.3 | Two element mesh distortion test

As shown in Figure 5, a cantilever beam is subjected to pure bending or end shear, which is often used to assess the distortion sensitivity of the quadrilateral plane elements. The geometry, material, and displacement boundary conditions are given in Figure 5. The beam is divided into two elements and the element distortion is characterized by the parameter δ varying from 0 to 4.9. The variations of displacement with mesh distortion under two load conditions are studied. The normalized lower tip deflections at endpoint A under two cases of loads are plotted in Figures 6A,B.

It can be seen that no matter how meshes are distorted, exact displacements under pure bending can be obtained by the present UQ6 element as shown in Figure 6A. The displacement by the present UQ6 lightly increases with the mesh distortion under the end shear load as shown in Figure 6B. It is also found that all unsymmetric elements give the same results in this test, while other typical incompatible and hybrid elements show obvious accuracy loss with mesh distortion.

TABLE 1 Results of the displacement at point A (Figure 4)

| α	u_A	v_A	$\sqrt{u^2 + v^2}$	Normalized
0°	−2.000000E+01	1.000000E+02	101.9804	1.0000
10°	−6.732051E+01	7.660254E+01	101.9804	1.0000
20°	−5.299587E+01	8.712886E+01	101.9804	1.0000
30°	−6.732051E+01	7.660254E+01	101.9804	1.0000
40°	−7.959965E+01	6.374869E+01	101.9804	1.0000
50°	−8.946020E+01	4.895787E+01	101.9804	1.0000
60°	−9.660254E+01	3.267949E+01	101.9804	1.0000
70°	−1.008097E+02	1.540816E+01	101.9804	1.0000
80°	−1.019537E+02	−2.331337E+00	101.9804	1.0000
90°	−1.000000E+02	2.000000E+01	101.9804	1.0000
Exact			101.9804	1.0000
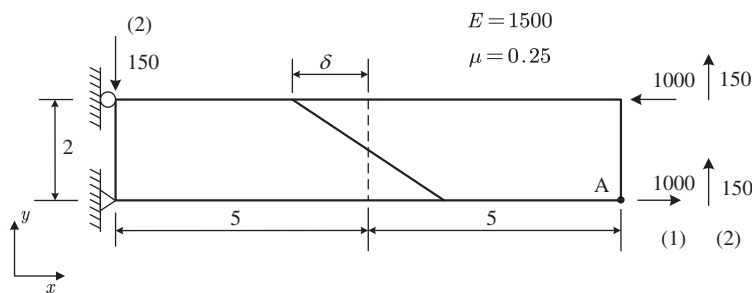
FIGURE 5 Distortion test of a two-element cantilever beam
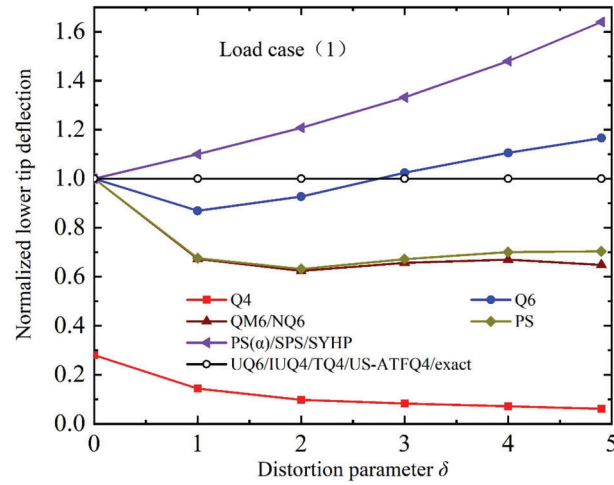
5.4 | Five-element cantilever beam

As shown in Figure 7, this problem involves a cantilever beam divided by five irregular quadrilateral elements under plane stress conditions subjected to two load cases. The lower tip deflections at point A as well as the normal stresses at point B are tabulated in Table 2 for the two load cases. The stress results by Q4/Q6/QM6/NQ6 are improved by bilinear extrapolation of the stresses at the Gaussian integration points. Unsurprisingly, the present element (as well as other unsymmetric elements) reproduces the exact solution under pure bending and yields very accurate solutions under end shear loading.

Different from traditional incompatible elements, the stresses are directly calculated without additional post-processing in the present element UQ6 since the quadratic completeness requirement in the physical space has been satisfied.

5.5 | MacNeal thin cantilever beam

As Figure 8 shown, a cantilever beam with a fully fixed end is subjected to a pure bending or shear load, and the beam is divided into three different mesh shapes: rectangle, parallelogram, and trapezoid. This test proposed by MacNeal and Harder[20] is a famous benchmark for investigating the sensitivity to mesh distortion. The Young's modulus is taken to be 10^7. Plane stress and plane strain is taken into consideration. The Poisson's ratio is equal to 0.3 in the plane stress condition. In plane strain condition, the Poisson's ratio is taken to be a varying value as 0.49 and 0.49999 to simulate the nearly impressible materials.

The results obtained by the present element UQ6 and other models in plane stress condition are summarized in Table 3. It can be seen that exact displacements under pure bending state and excellent results under end shearing load
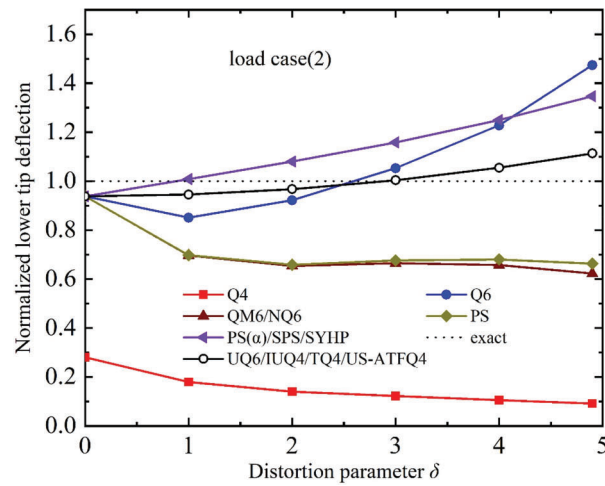
FIGURE 6 Normalized lower tip deflection at point A (Figure 5)

FIGURE 7 Five-element cantilever beam under pure bending and shearing

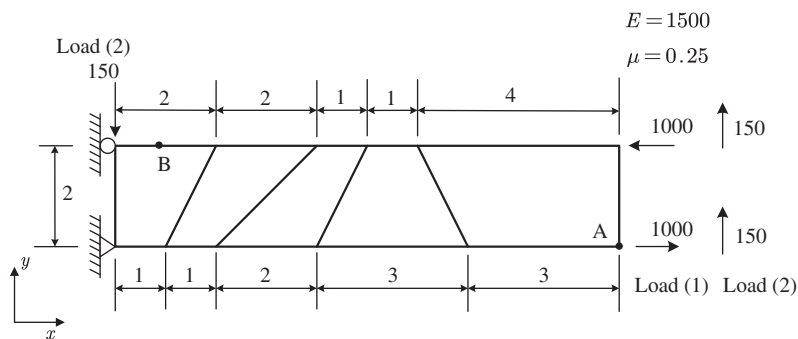**TABLE 2** Deflections and stresses of the cantilever beam (Figure 7)

Element	Load (1)		Load (2)	
	v_A	σ_{xB}	v_A	σ_{xB}
Q4	45.7	−2111	50.7	−2939
Q6	98.4	−3002	100.4	−4159
QM6/NQ6	96.1	−3014	98.1	−4137
PS	96.2	−3014	98.2	−4137
PS (α)	100.4	−3000	100.9	−4125
SPS/SYHP	102.1	−3000	101.3	−4126
UQ6/IUQ4/TQ4/US-ATFQ4	**100.0**	**−3000**	**101.5**	**−4125**
Exact	100.0	−3000	102.6	−4050

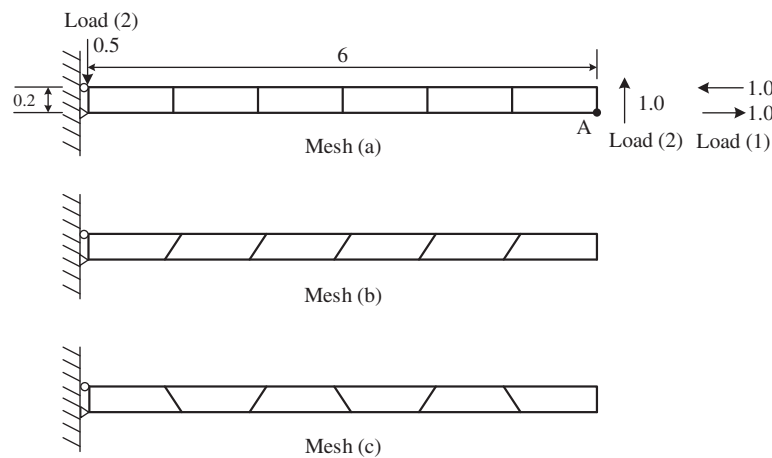*Note*: The bold values are computed by the present method.

FIGURE 8 MacNeal's thin cantilever with regular and irregular meshes

can be obtained by the UQ6 element. Therefore, the present element UQ6 is free of trapezoidal locking and insensitive to mesh distortion under plane stress assumption. Obviously, all the four-node unsymmetric elements developed by Cen et al.,[6] Xie et al.,[8] and Huang et al.[11] can pass the benchmark test, while the typical incompatible and hybrid elements including the PS/Q6/QM6/NQ6 elements fail with locking.

Table 4 shows the normalized results of the upper tip deflections of the MacNeal thin cantilever under the two load cases with plane strain assumption. When the Poisson's ratio is extremely close to 0.5, which represents the incompressible state of a material, the UQ6 element still exhibits excellent performance and is free of volumetric locking regardless of the meshes and loading cases. It is also found that severe volume locking exists in the Q4 element, and the Q6/PS/QM6/NQ6 elements are only free of locking with regular mesh. The PS(α)/SPS/SYHP elements can pass the volume locking test in nearly incompressible conditions with all meshes.

6 | NUMERICAL TESTS FOR THE 3D ELEMENT UH11

In this section, some benchmark problems are chosen to investigate the performance of the present element UH11. Some typical eight-node hexahedral elements are selected and listed below for comparison:

UH11: present unsymmetric element.
H8: Standard isoparametric element.
H11: Incompatible element by Wilson et al.[15]
NH11: Incompatible element by Wu et al.[13]

TABLE 3 Normalized upper tip deflections of the MacNeal thin cantilever under two load cases with plane stress assumption (Figure 8)

Element	Load (1)			Load (2)		
	Mesh (a)	(b)	(c)	Mesh (a)	(b)	(c)
Q4	0.093	0.023	0.031	0.093	0.028	0.035
Q6	1.000	0.238	0.912	0.993	0.299	0.883
PS/QM6/NQ6	1.000	0.165	0.844	0.993	0.221	0.796
PS(α)	1.000	1.027	0.994	0.993	1.013	0.989
SPS/SYHP	1.000	1.022	0.994	0.993	1.009	0.989
UQ6/IUQ4/TQ4/US-ATFQ4	**1.000**	**1.000**	**1.000**	**0.993**	**0.994**	**0.993**
Exact[a]	1.000			1.000		

Note: The bold values are computed by the present method.

[a]The exact solutions of load (1) and (2) are 0.0054 and 0.1081, respectively.

TABLE 4 Upper tip deflections of the MacNeal thin cantilever under two load cases with plane strain assumption (Figure 8)

Element	Mesh	Load (1)		Load (2)	
		$\mu = 0.49$	$\mu = 0.49999$	$\mu = 0.49$	$\mu = 0.49999$
Q4	a	0.052	0.000	0.052	0.001
	b	0.019	0.010	0.022	0.010
	c	0.012	0.001	0.016	0.003
Q6	a	1.000	1.000	0.993	0.993
	b	0.239	0.238	0.299	0.299
	c	0.913	0.912	0.883	0.883
PS/QM6/NQ6	a	1.000	1.000	0.993	0.993
	b	0.170	0.171	0.227	0.227
	c	0.848	0.847	0.800	0.800
PS(α)	a	1.000	1.000	0.993	0.993
	b	1.028	1.027	1.013	1.013
	c	0.995	0.995	0.989	0.989
SPS/SYHP	a	1.000	1.000	0.993	0.993
	b	1.022	1.021	1.009	1.008
	c	0.995	0.995	0.989	0.989
UQ6/IUQ4/TQ4/US-ATFQ4	a	**1.000**	**1.000**	**0.993**	**0.993**
	b	**1.000**	**1.000**	**0.993**	**0.993**
	c	**1.000**	**1.000**	**0.993**	**0.993**
Exact[a]		1.000	1.000	1.000	1.000

Note: The bold values are computed by the present method.

[a]The exact solutions are 0.00410, 0.00405, 0.08217, and 0.08110, respectively.

PT: Hybrid-stress element by Pian and Tong.[21]

OPH-18β: Hybrid stress hexahedral element by Wu et al.[13]

OPH-18$\beta(\alpha)$: Hybrid stress element optimized by penalty equilibrium by Wu et al.[13]

TH8: Unsymmetric element with adjustable factor β (0.01 or 0.0001) by Xie et al.[8]

US-ATFH8: Unsymmetric element using Airy stress solution by Zhou et al.[7]

6.1 | Patch test

The solid patch test[20] is considered as shown in Figure 9. The unit cube is divided by seven arbitrary distorted elements and the locations of inner nodes are listed in Figure 9. The displacement boundary conditions corresponding to constant strains are:

$$u = 10^{-3}(2x + y + z)/2$$
$$v = 10^{-3}(x + 2y + z)/2$$
$$w = 10^{-3}(x + y + 2z)/2 \tag{36}$$

And the stress solutions are:

$$\sigma_x = \sigma_y = \sigma_z = 2000; \tau_{xy} = \tau_{yz} = \tau_{zx} = 400 \tag{37}$$

In the test, the displacement constraints calculated in (36) are applied to all boundary nodes. The present element UH11 is able to reproduce the exact solution, which shows that it strictly passes the patch test. Furthermore, the internal node 1 is re-located to (0.780, 0.690, 0.640) which is very close to the internal node 7. In this case with severely distorted patch, the UH11 element can also pass the constant stress test without difficulty.

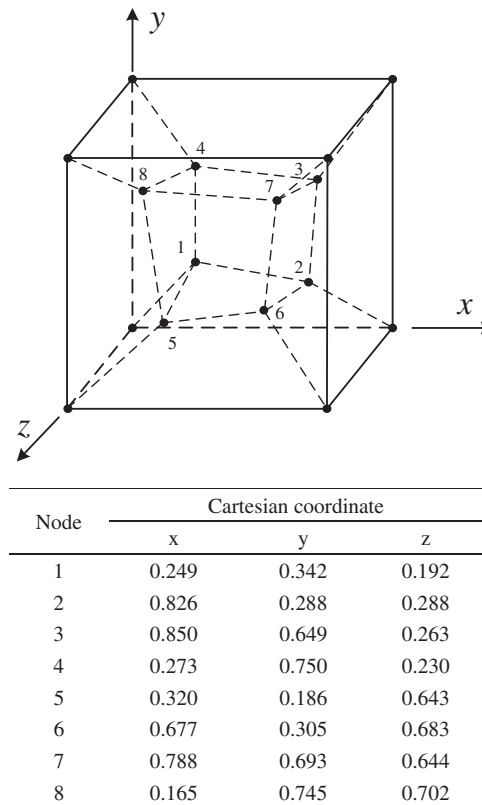| Node	Cartesian coordinate		
	x	y	z
1	0.249	0.342	0.192
2	0.826	0.288	0.288
3	0.850	0.649	0.263
4	0.273	0.750	0.230
5	0.320	0.186	0.643
6	0.677	0.305	0.683
7	0.788	0.693	0.644
8	0.165	0.745	0.702

FIGURE 9 Patch test; outer dimensions: unit cube; $E = 10^6$; $\mu = 0.25$

6.2 | Rotational frame dependence test

To test whether the UH11 element is invariant and isotropic, the geometry used by Zhou et al.[7] is considered. As shown in Figure 10, the $10 \times 5 \times 1$ cantilever beam subjected to a pure bending moment is divided into two distorted elements. The Young's modulus $E = 100.0$, and the Poisson ratio $\mu = 0.3$. The Cartesian coordinate system rotates counterclockwise from $\alpha_1 = 0°$ to $90°$ in steps of $15°$ around the z-axis. Three positions of the model ($\alpha_1 = 30°, \alpha_2 = 60°, \alpha_3 = 90°; \alpha_1 = \alpha_2 = \alpha_3 = 45°; \alpha_1 = \alpha_2 = 90°$) are selected to prove that it is invariant and isotropic in all axes, where α_2, α_3 are the angles around the y-axis and the x-axis, respectively.

The magnitude of displacement $\sqrt{u^2 + v^2 + w^2}$ is calculated to test its variance and the normalized results are listed in Table 5. As a reference, the 'overkill solution' is computed by using 50,000 20-node hexahedral isoparametric elements of Abaqus.[7] It is noted that the same results are obtained at all rotation angles, which shows the present element UH11 is invariant and isotropic.

6.3 | Cheung and Chen beam tests

It is fundamental and crucial to evaluate the sensitivity of elements to distorted meshes. This test was originally proposed by Cheung and Chen[22] for testing the sensitivity to distortion of the 8-node hexahedral element. As shown in Figure 11, the $10 \times 2 \times 2$ cantilever beam subjected to a pure bending moment M or a transverse shear force P is discretized into 12 meshes and the x coordinates of nodes 1, 2, 3, and 4 in the Meshes (2) to (10) are listed in Table 6. The
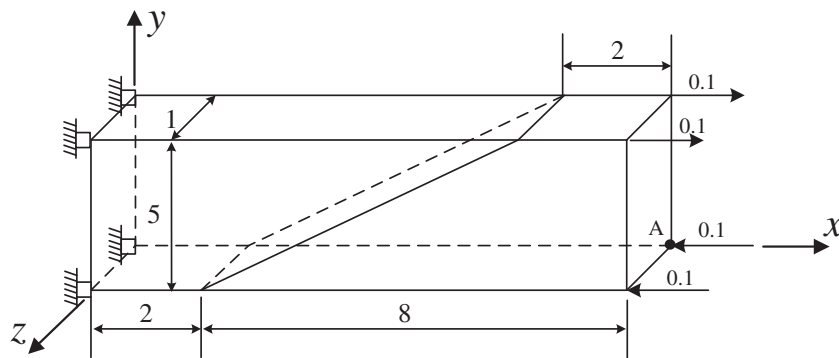

FIGURE 10 Rotation dependence test for solid elements

TABLE 5 Results of the displacement at point A (Figure 10)

α_1	α_2	α_3	u_A	v_A	w_A	$\sqrt{u_A^2 + v_A^2 + w_A^2}$	Normalized
0°			−2.383673E-02	−4.618922E-02	−3.325401E-04	5.1978305E-02	0.97773
15°			−1.106986E-02	−5.078476E-02	−3.325401E-04	5.1978305E-02	0.97773
30°			2.451398E-03	−5.191941E-02	−3.325401E-04	5.1978312E-02	0.97773
30°	60°	90°	9.377108E-04	2.289243E-03	−5.191941E-02	5.1978312E-02	0.97773
45°			1.580560E-02	4.951583E-02	−3.325401E-04	5.1978312E-02	0.97773
45°	45°	45°	1.094111E-02	−2.694391E-02	−4.308205E-02	5.1978316E-02	0.97773
60°			2.808268E-02	−4.373783E-02	−3.325401E-04	5.1978312E-02	0.97773
75°			3.844596E-02	−3.497916E-02	−3.325401E-04	5.1978305E-02	0.97773
90°			4.618922E-02	−2.383673E-02	−3.325401E-04	5.1978305E-02	0.97773
90°	90°		−3.325401E-04	−2.383673E-02	−4.618922E-02	5.1978305E-02	0.97773
Overkill solution						0.053162	1.00000
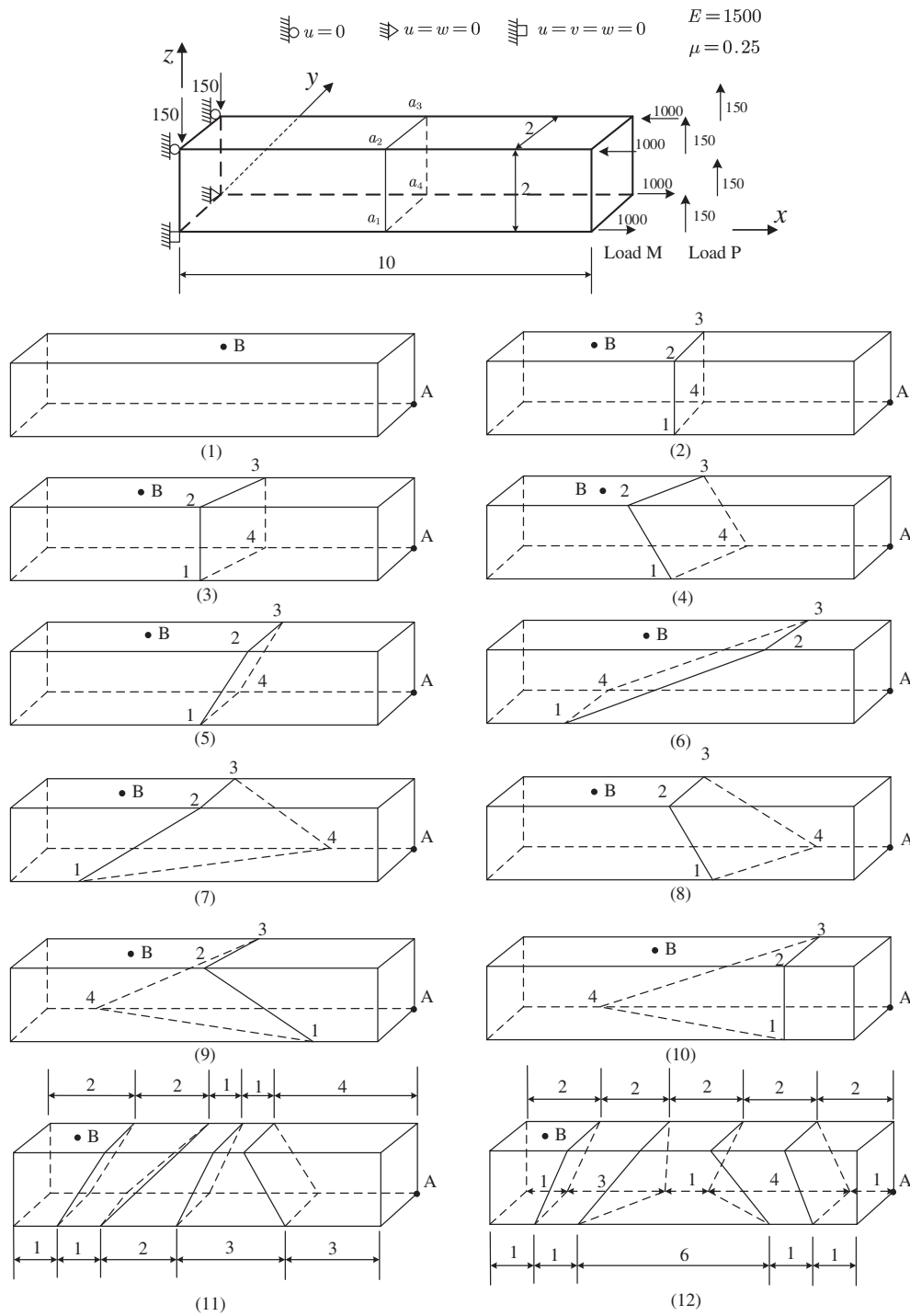
FIGURE 11 Cheng and Chen beam tests

TABLE 6 The x coordinates of nodes 1, 2, 3, and 4 in meshes 2 to 10 (Figure 11)

x-coordinates	Mesh								
	(2)	**(3)**	**(4)**	**(5)**	**(6)**	**(7)**	**(8)**	**(9)**	**(10)**
x_1	5	5	5	5	2	2	6	8	8
x_2	5	5	4	6	8	5	5	5	8
x_3	5	5	5	6	8	5	5	6	8
x_4	5	6	6	5	2	8	8	2	2

meshes are distorted from the original regular mesh into the severely distorted forms. The Young's modulus $E = 1500$ and the Poisson's ratio $\mu = 0.25$. The normalized end deflection at point A as well as the results of stress at point B are computed and listed in Tables 7 and 8, respectively. The stress results are directly computed without post-process or tri-linear extrapolation.

It is noted that the exact solutions under pure bending are obtained by the present UH11 element no matter how severe the mesh distortion is. Under the shearing load, the results yielded by the UH11 element are relatively accurate and stable in all mesh cases.

Under both load cases, the results obtained by the UH11 element are very close to the other two unsymmetric elements TH8 and US-ATFH8. They are more accurate than those by the typical incompatible and hybrid elements, which indicates the advantages of the unsymmetric FEM. With the Mesh (12) under load P, wrong displacement results may appear for the TH8 element. It indicates that the TH8 element is affected by the adjustable factor β in some cases. The results of the standard isoparametric element H8 are far less accurate than other elements. The hybrid stress element OPH-18$\beta(\alpha)$ optimized by the penalty equilibrium method has acceptable displacement results and gains more accurate stress solutions than others in most cases. However, it gives poor displacement results in the Meshes (6), (9), and (10).

TABLE 7 Normalized tip deflection at point A for Cheung and Chen tests (Figure 11)

Mesh	H8	H11	NH11	PT	OPH-18 β	OPH-18 $\beta(\alpha)$	TH8 $\beta = 0.01$	TH8 $\beta = 0.0001$	US-ATFH8	UH11
Load M: normalized deflections at point A (the exact solution is 100)										
1	0.0901	1.0000	1.0000	1.0000	1.0000	1.0000	1.0000	1.0000	1.0000	**1.0000**
2	0.2778	1.0000	1.0000	1.0000	1.0000	1.0000	1.0000	1.0000	1.0000	**1.0000**
3	0.2352	0.9397	0.8937	0.9227	0.9232	1.0213	1.0000	1.0000	1.0000	**1.0000**
4	0.2027	0.8962	0.7907	0.8135	0.8172	1.0707	1.0000	1.0000	1.0000	**1.0000**
5	0.1881	0.8836	0.7716	0.7720	0.7720	0.9475	1.0000	1.0000	1.0000	**1.0000**
6	0.0826	0.7875	0.4074	0.4136	0.4136	0.6670	1.0000	1.0000	1.0000	**1.0000**
7	0.1270	0.5126	0.4667	0.3219	0.3228	1.2211	1.0000	1.0000	1.0000	**1.0000**
8	0.1230	0.8312	0.6594	0.6633	0.6441	1.1792	1.0000	1.0000	1.0000	**1.0000**
9	0.1071	0.3967	0.3494	0.2255	0.2252	0.7361	1.0000	1.0000	1.0000	**1.0000**
10	0.0850	0.3398	0.2501	0.3295	0.2926	0.6175	1.0000	1.0000	1.0000	**1.0000**
11	0.4438	0.9826	0.9580	0.9594	0.9594	0.9986	1.0000	1.0000	1.0000	**1.0000**
12	0.3991	0.7716	0.7150	0.7676	0.7783	0.8983	1.0000	1.0000	1.0000	**1.0000**
Load P: normalized deflections at point A (the exact solution is 102.6)										
1	0.0902	0.7554	0.7554	0.7554	0.7554	0.7554	0.7554	0.7554	0.7554	**0.7554**
2	0.2778	0.9340	0.9340	0.9353	0.9353	0.9353	0.9380	0.9381	0.9340	**0.9340**
3	0.2347	0.8773	0.8437	0.8756	0.8745	0.9497	0.9370	0.9358	0.9262	**0.9252**
4	0.2223	0.8479	0.7685	0.7959	0.7974	0.9868	0.9378	0.9369	0.9270	**0.9257**
5	0.2024	0.8491	0.7646	0.7660	0.7660	0.8944	0.9380	0.9381	0.9343	**0.9341**
6	0.1213	0.8723	0.4788	0.4850	0.4850	0.6702	1.0038	1.0039	1.0135	**0.9968**
7	0.1634	0.4926	0.4587	0.4068	0.4064	1.0913	0.8595	0.8586	0.8615	**0.8921**
8	0.1510	0.8051	0.6697	0.6848	0.6692	1.0585	0.9534	0.9503	0.9929	**0.9553**
9	0.1460	0.4064	0.3718	0.3361	0.3349	0.7384	0.8074	0.8028	0.9026	**0.8700**
10	0.1160	0.3316	0.2694	0.3624	0.3341	0.6376	0.7550	0.7541	0.7062	**0.7707**
11	0.4808	0.9770	0.9538	0.9552	0.9552	0.9813	0.9889	0.9889	0.9875	**0.9876**
12	0.4531	0.8061	0.7580	0.8065	0.8136	0.8984	0.9618	−2.6592	0.9926	**0.9896**

Note: The bold values are computed by the present method.

TABLE 8 The results of stress at point B for Cheung and Chen tests (Figure 11)

Mesh	H8	H11	NH11	PT	OPH-18 β	OPH-18 $\beta(\alpha)$	TH8 $\beta = 0.01$	US-ATFH8	UH11	Exact
Load M										
1	−297	−3000	−3000	−3000	−3000	−3000	−3000	−3000	**−3000**	−3000
2	−917	−3000	−3000	−3000	−3000	−3000	−3000	−3000	**−3000**	−3000
3	−706	−2775	−2623	−2714	−2715	−2988	−3000	−3000	**−3000**	−3000
4	−697	−3155	−2756	−2404	−2415	−2985	−3000	−3000	**−3000**	−3000
5	−586	−2251	−1967	−2348	−2348	−2989	−3000	−3000	**−3000**	−3000
6	−129	−241	399	−1343	−1343	−2993	−3000	−3000	**−3000**	−3000
7	−399	−1348	−1213	−859	−861	−2977	−3000	−3000	**−3000**	−3000
8	−449	−3580	−2865	−2047	−1985	−2995	−3000	−3000	**−3000**	−3000
9	−326	−1079	−969	−672	−704	−2982	−3000	−3000	**−3000**	−3000
10	−179	−548	−336	−1044	−910	−2986	−3000	−3000	**−3000**	−3000
11	−1736	−2340	−2353	−3015	−3015	−3000	−3000	−3000	**−3000**	−3000
12	−1738	−2303	−2273	−2956	−2958	−3001	−3000	−3000	**−3000**	−3000
Load P										
1	−223	−2250	−2250	−2250	−2250	−2250	−2250	−2250	**−2250**	−2250
2	−1037	−3375	−3375	−3375	−3375	−3375	−3375	−3375	**−3375**	−3375
3	−806	−3037	−2923	−3032	−3031	−3243	−3257	−3230	**−3222**	−3263
4	−903	−3655	−3347	−2947	−2954	−3393	−3409	−3373	**−3361**	−3375
5	−694	−2518	−2300	−2736	−2736	−3217	−3225	−3227	**−3225**	−3150
6	−243	−210	193	−1907	−1907	−3145	−3150	−3199	**−3150**	−2700
7	−665	−1720	−1617	−1610	−1630	−3354	−2884	−3039	**−3162**	−3375
8	−638	−3975	−3398	−2521	−2474	−3219	−3240	−3370	**−3245**	−3375
9	−566	−1392	−1311	−1431	−1464	−3285	−2695	−3083	**−2996**	−3263
10	−292	−588	−465	−1262	−1177	−2911	−2276	−2171	**−2343**	−2700
11	−2415	−3234	−3221	−4139	−4139	−4125	−4125	−4125	**−4125**	−4050
12	−2419	−3180	−3118	−4060	−4062	−4126	−4123	−4125	**−4123**	−4050

Note: The bold values are computed by the present method.

6.4 | Two-element 3D cantilever

The $10 \times 2 \times 2$ cantilever commonly adopted to examine the sensitivity to mesh distortion of the 8-node hexahedral element is shown in Figure 12. The cantilever beam is divided by two elements containing a parameter of distortion δ and it is subjected to a pure bending moment M or transverse force P. The distortion parameter δ varies from 0 to 4.9, which indicates the mesh changes from a rectangular division to a severely distorted division. The material parameters are given in Figure 12. The normalized results of the vertical deflection at point A and stress σ_{xB} at point B under the two load cases are presented in Figures 13 and 14, respectively.

The present element UH11 as well as other unsymmetric elements can reproduce the exact solution regardless of distortions under pure bending. Furthermore, the results of the UH11 element under shearing load are either comparable or better than those of other elements. The unsymmetric element US-ATFH8 presents better stress solutions for shearing load, while the present element UH11 yields better displacement prediction than US-ATFH8.
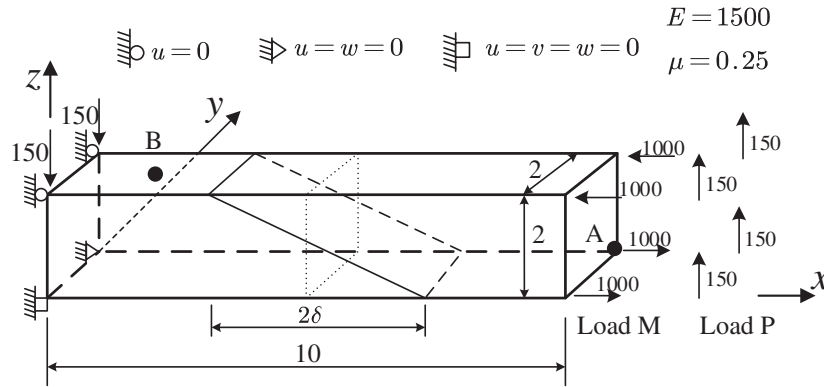
FIGURE 12 A two-element cantilever subjected to bending load M and shearing load P with mesh distortion
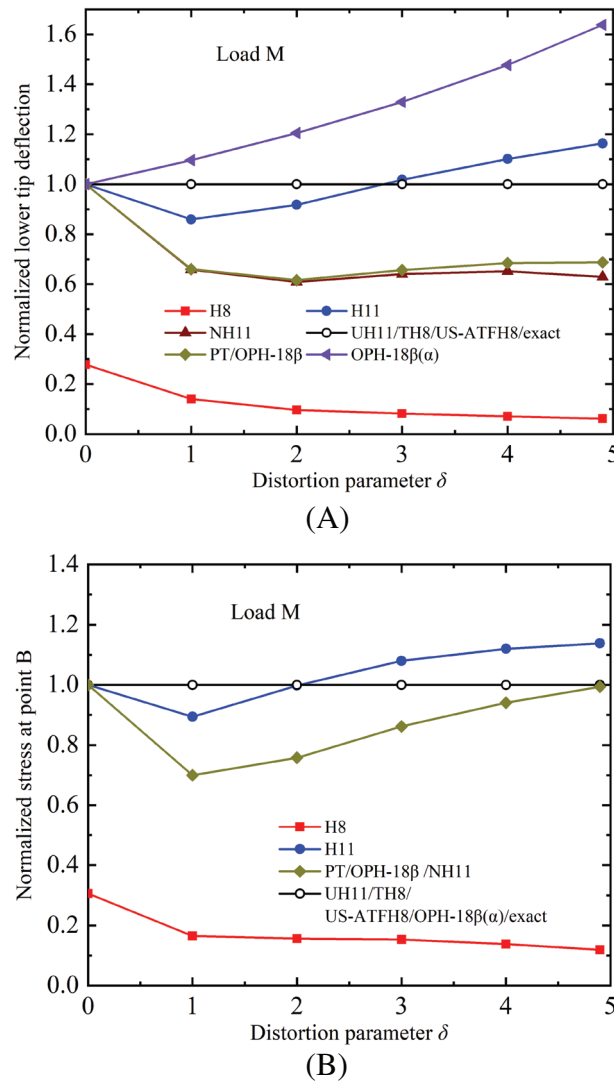

FIGURE 13 Normalized deflection at point A and stress σ_{xB} at point B under pure bending
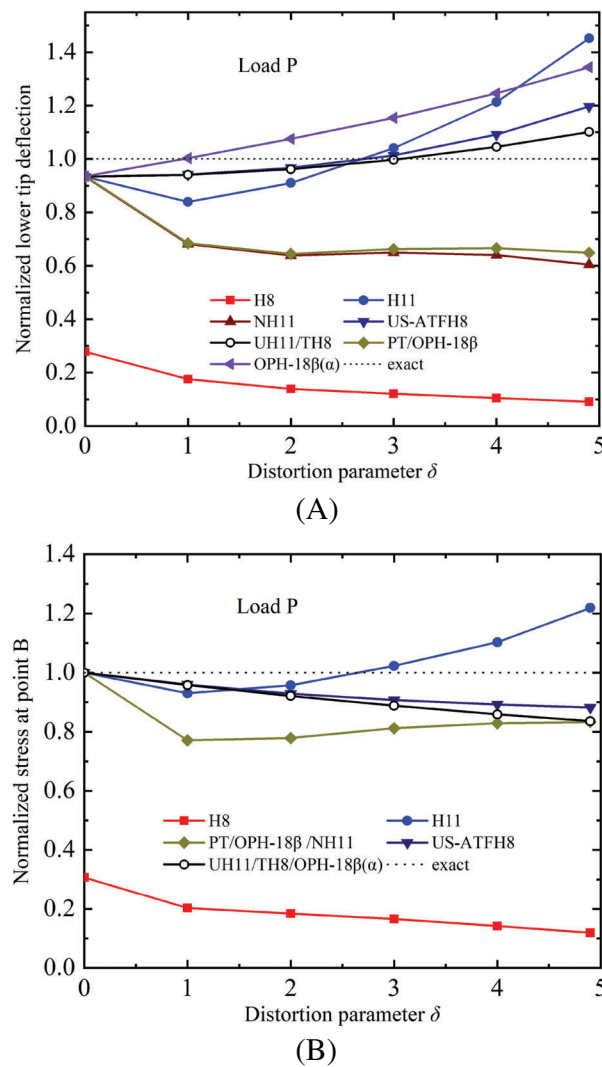
FIGURE 14   Normalized deflection at point A and stress σ_{xB} at point B under pure shearing

6.5 | Cook's skew beam problem

The Cook's skew beam problem proposed by Cook[23] is repeated by the present element UH11 to test its convergence. As shown in Figure 15, a skew cantilever subjected to shear uniformly distributed load at the free edge is divided into meshes with different densities (from $2 \times 2 \times 2$ to $16 \times 16 \times 16$). The geometry and material constants of the beam are also given in the figure. The results of vertical deflection at point A are listed in Table 9, which demonstrates that the present element UH11 has excellent convergence. The reference solution is 23.86[7] which is obtained by 20-node hexahedral isoparametric elements using $46 \times 46 \times 46$ mesh in Abaqus.

Generally, the unsymmetric elements are more expensive than traditional symmetric ones due to more computer memory for storage and more time cost for computations. In our program, an unsymmetric frontal solver is adopted and therefore no significant increase of the memory storage. The computation time cost in seconds for the $16 \times 16 \times 16$ mesh with total 4913 nodes is given in Table 9. The results are obtained using a PC under Windows system. It is shown that the unsymmetric elements take about 0.08% more time per node than symmetric ones. Further studies show that the additional time is mainly taken on solving the equilibrium equations.

6.6 | Bending of a thin curved beam

As shown in Figure 16, the thin curved beam with a fully fixed end is subjected to two cases of shearing load (in-plane shear or out-plane shear at its tip), respectively. The inner radius R_i, thickness h and width t of the beam are 4.12, 0.2, and
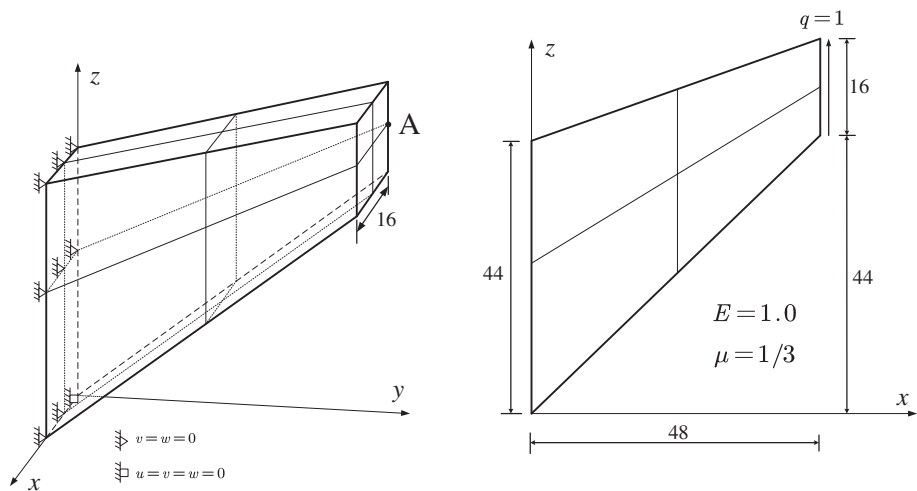
FIGURE 15 Cook's skew beam problem

TABLE 9 The results of vertical deflection at point A (Figure 15)

Element	$2 \times 2 \times 2$	$4 \times 4 \times 4$	$8 \times 8 \times 8$	$16 \times 16 \times 16$	Time cost
H8	11.35	17.65	21.71	23.18	69.27
H11	22.65	23.28	23.68	23.83	71.08
NH11	20.83	22.85	23.57	23.78	69.69
PT	20.94	22.86	23.58	23.82	69.99
TH8 β=0.01	22.59	23.27	23.67	23.81	349.83
US-ATFH8	22.56	23.27	23.67	23.81	348.81
UH11	**22.57**	**23.27**	**23.67**	**23.81**	348.75

Note: The bold values are computed by the present method.
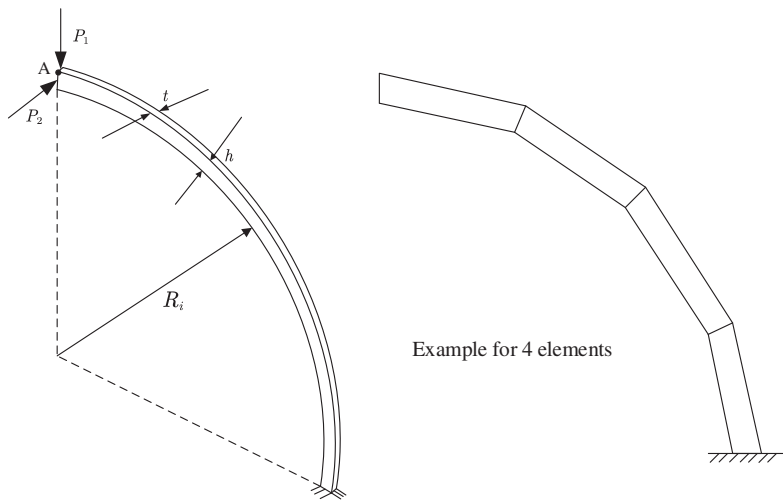

FIGURE 16 Bending of a thin curved beam

0.1, respectively. The material parameters are $E = 1 \times 10^7$ and $\mu = 0.3$. The results of the deflection at point A are listed in Table 10. It is obvious that the present element UH11 exhibits great convergence.
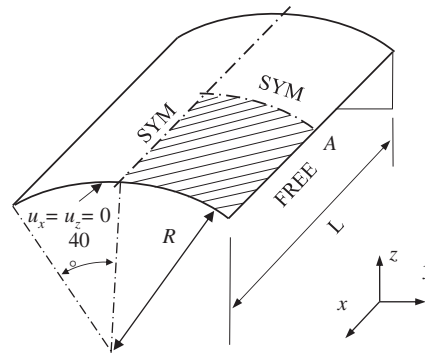
6.7 | Scordelis-Lo roof with self-weight

The Scordelis-Lo roof problem is also a proposed standard test[20] for solid and shell elements. Details of the roof's geometry, constraints, and material properties are shown in Figure 17. The shell is supported on the curved edges and loaded by its weight with 90 per mid-surface area. Due to symmetry, only a quarter of the roof (the shaded area shown in Figure 17) is discretized. The vertical deflection at the midpoint A of the free edge is computed and normalized by the reference value 0.3024.[20] The results are presented in Table 11 with different N × N divisions of the shell surface. It is found that the present element exhibits no superiority over traditional symmetric incompatible elements H11 and NH11. The hybrid stress element PT and the unsymmetric element TH8 with a scaled factor 0.01 provide better numerical accuracy with coarse meshes. The OPH-18β element fails in this test due to hourglass modes. The reason for this can be explained by looking into the assumed trial displacements in Equation (33) in which the incomplete cubic term $\overline{xyz}$ is introduced. The resulted incomplete quadratic shear strains/stresses restrict the deformation of elements. The TH8 element reduces the effect of the cubic term by scaling its contributions and the PT element adopts the assumed optimized stress field with linear shear stresses. The present unsymmetric element UH11 can also be well improved in this example by not considering the cubic term when the shear strains are evaluated, or by scaling the same as the TH8 element. However, further investigations are needed to develop the unsymmetric shell elements without shear locking based on the shell theory assumptions.

TABLE 10 Normalized deflection at point A for a thin curved beam (Figure 16)

Elements	H8	H11	NH11	PT	OPH-18 β	OPH-18 $\beta(\alpha)$	TH8 β=0.01	US-ATFH8	UH11
In-plane shear P$_1$ (standard solution is 0.08734[7])									
2	0.006	0.104	0.048	0.048	0.048	0.583	0.947	0.909	**0.909**
4	0.033	0.710	0.574	0.575	0.575	0.925	0.991	0.974	**0.974**
6	0.076	0.931	0.876	0.877	0.877	0.974	1.002	0.992	**0.992**
8	0.128	0.981	0.960	0.961	0.961	0.991	1.006	0.999	**0.999**
10	0.187	0.996	0.987	0.988	0.988	0.998	1.009	1.003	**1.003**
12	0.248	1.002	0.997	0.998	0.998	1.002	1.010	1.005	**1.005**
14	0.307	1.005	1.002	1.003	1.003	1.005	1.011	1.007	**1.007**
16	0.364	1.007	1.005	1.005	1.005	1.006	1.011	1.008	**1.008**
18	0.417	1.008	1.007	1.007	1.007	1.008	1.012	1.009	**1.009**
20	0.464	1.009	1.008	1.009	1.009	1.009	1.012	1.009	**1.009**
Out-of-plane shear P$_2$ (standard solution is 0.5022[7])									
2	0.131	0.197	0.161	0.190	0.200	0.609	0.896	0.968	**0.885**
4	0.207	0.678	0.581	0.614	0.621	0.918	0.952	0.934	**0.915**
6	0.237	0.873	0.829	0.857	0.861	0.956	0.964	0.945	**0.937**
8	0.258	0.925	0.908	0.929	0.932	0.967	0.969	0.952	**0.947**
10	0.277	0.944	0.936	0.952	0.954	0.971	0.972	0.956	**0.953**
12	0.296	0.952	0.948	0.962	0.962	0.974	0.973	0.960	**0.957**
14	0.316	0.957	0.955	0.966	0.966	0.975	0.974	0.962	**0.960**
16	0.337	0.960	0.959	0.968	0.968	0.976	0.975	0.964	**0.962**
18	0.358	0.963	0.962	0.970	0.970	0.976	0.975	0.965	**0.964**
20	0.379	0.964	0.963	0.970	0.971	0.976	0.976	0.966	**0.965**

Note: The bold values are computed by the present method.

$R{=}25$, $L{=}50$, $h{=}0.25$, $E{=}4.32{\times}\,10^{8}$, $\mu=0$, self-weight 90/area

FIGURE 17 Scordelis-Lo roof

TABLE 11 Normalized vertical deflection at midpoint of the free edge

Element	4×4	8×8	16×16
H8	0.0624	0.1232	0.2620
H11	0.5508	0.9573	1.0020
NH11	0.5469	0.9567	1.0019
PT	1.0374	1.0126	1.0057
OPH-18β	Failed		
TH8 $\beta = 0.01$	1.0542	1.0143	1.0061
US-ATFH8	0.5554	0.9578	1.0022
UH11	**0.5555**	**0.9579**	**1.0022**

Note: The bold values are computed by the present method.

7 | CONCLUSIONS

In this article, by introducing Wilson's incompatible functions to the standard isoparametric test functions and adding internal nodes to form the trial functions, novel incompatible unsymmetric 4-node quadrilateral plane element UQ6 and 8-node hexahedral solid element UH11 are successfully developed, which can be taken as the straightforward extensions of Wilson's incompatible elements to their unsymmetric forms.

The introduction of incompatible displacement with the satisfaction of the patch test condition releases the inter-element continuity requirement of the virtual displacements. It also provides a way to develop low-order unsymmetric elements with high numerical accuracy and distortion resistance. The trial functions established in the local skew frame attached to the element central avoid the rotational variance. Furthermore, by introducing local area/volume coordinates and careful selection of internal nodes, the explicit expressions of the trial shape functions can be obtained without matrix inversion. This technique is very useful to develop high-order unsymmetric elements.

Numerical results demonstrate that both the UQ6 and UH11 elements are immune to various severe mesh distortion, rotational frame invariant, free of MacNeal trapezoidal locking, and incompressible volumetric locking in contrast with traditional symmetric elements. Though the numerical performances of the present elements are similar to that of other unsymmetric elements based on analytic stress solutions, the present method is more applicable and more convenient to be extended to other physical problems. Furthermore, the present elements can take less additional computational cost by explicit computation and static condensation. It is also found that the present UH11 element exhibits no advantages over symmetric incompatible and hybrid stress elements in the analysis of thin shell problems.

DATA AVAILABILITY STATEMENT

The data that support the findings of this study are available from the corresponding author upon reasonable request.

ORCID

Ying-Qing Huang https://orcid.org/0000-0002-2373-7684

REFERENCES

1. Rajendran S, Liew KM. A novel unsymmetric 8-node plane element immune to mesh distortion under a quadratic displacement field. *Int J Numer Methods Eng*. 2003;58(11):1713-1748.
2. Rajendran S. A technique to develop mesh-distortion immune finite elements. *Comput Methods Appl Mech Eng*. 2010;199(17–20):1044-1063.
3. Liew KM, Rajendran S, Wang J. A quadratic plane triangular element immune to quadratic mesh distortions under quadratic displacement fields. *Comput Methods Appl Mech Eng*. 2006;195(9–12):1207-1223.
4. Ooi ET, Rajendran S, Yeo JH. A 20-node hexahedron element with enhanced distortion tolerance. *Int J Numer Methods Eng*. 2004;60(15):2501-2530.
5. Cen S, Zhou GH, Fu XR. A shape-free 8-node plane element unsymmetric analytical trial function method. *Int J Numer Methods Eng*. 2012;91(2):158-185.
6. Cen S, Zhou PL, Li CF, Wu CJ. An unsymmetric 4-node, 8-DOF plane membrane element perfectly breaking through MacNeal's theorem. *Int J Numer Methods Eng*. 2015;103(7):469-500.
7. Zhou PL, Cen S, Huang JB, Li CF, Zhang Q. An unsymmetric 8-node hexahedral element with high distortion tolerance. *Int J Numer Methods Eng*. 2017;109(8):1130-1158.
8. Xie Q, Sze KY, Zhou YX. Modified and Trefftz unsymmetric finite element models. *Int J Mech Mater Des*. 2016;12(1):53-70.
9. Shang Y, Ouyang W. 4-node unsymmetric quadrilateral membrane element with drilling DOFs insensitive to severe mesh-distortion. *Int J Numer Methods Eng*. 2018;113:1589-1606.
10. Shang Y, Qian ZH, Cen S, Li CF. A simple unsymmetric 4-node 12-DOF membrane element for the modified couple stress theory. *Int J Numer Methods Eng*. 2019;119:807-825.
11. Huang YQ, Huan YK, Chen HB. An incompatible and unsymmetric four-node quadrilateral plane element with high numerical performance. *Int J Numer Methods Eng*. 2020;121(15):3382-3396.
12. Yuan KY, Huang YS, Pian THH. New strategy for assumed stresses for 4-node hybrid stress membrane element. *Int J Numer Methods Eng*. 1993;36(10):1747-1763.
13. Wu CC, Huang MG, Pian THH. Consistency condition and convergence criteria of incompatible elements: general formulation of incompatible functions and its application. *Comput Struct*. 1987;27(5):639-644.
14. Huang YQ, Li QS. Four-node incompatible plane and axisymmetric elements with quadratic completeness in the physical space. *Int J Numer Methods Eng*. 2004;61:1603-1624.
15. Wilson EL, Taylor RL, Doherty WP, Ghabussi T. Incompatible displacement models. In: Fenven ST, ed. *Numerical and Computer Methods in Structural Mechanics*. Academic Press; 1973.
16. Taylor RL, Beresford PJ, Wilson EL. A non-conforming element for stress analysis. *Int J Numer Methods Eng*. 1976;10(6):1211-1219.
17. Pian THH, Sumihara K. Rational approach for assumed stress finite elements. *Int J Numer Methods Eng*. 1984;20(9):1685-1695.
18. Wu CC, Cheung YK. On optimization approaches of hybrid stress elements. *Finite Elem Anal Des*. 1995;21:111-128.
19. Sze KY. On immunizing five-beta hybrid stress element models from 'trapezoidal locking' in practical analyses. *Int J Numer Methods Eng*. 2000;47(4):907-920.
20. MacNeal RH, Harder RL. A proposed standard set of problems to test finite element accuracy. *Finite Elem Anal Des*. 1985;1:3-20.
21. Pian THH, Tong P. Relations between incompatible model and hybrid stress model. *Int J Numer Methods Eng*. 1986;22(1):173-181.
22. Cheung YK, Chen WJ. Isoparametric hybrid hexahedral elements for three dimensional stress analysis. *Int J Numer Methods Eng*. 1988;26(3):677-693.
23. Cook RD, Malkus DS, Plesha ME. *Concepts and Applications of Finite Element Analysis*. 3rd ed. John Wiley & Sons, Inc; 1989.

How to cite this article: Huang Y-Q, Yang Y-F, Wang J-Z, Liu X-C, Chen H-B. Unsymmetric extensions of Wilson's incompatible four-node quadrilateral and eight-node hexahedral elements. *Int J Numer Methods Eng*. 2022;123(1):101-127. doi: 10.1002/nme.6849